Optics Communications 381 (2016) 336–345

Contents lists available at ScienceDirect

Optics Communications

journal homepage: www.elsevier.com/locate/optcom

Refractive index and surface roughness estimation using passive multispectral and multiangular polarimetric measurements

Bin Yang [a,b,*], Changxiang Yan [a], Junqiang Zhang [a], Haiyang Zhang [a,b]

[a] Changchun Institute of Optics, Fine Mechanics and Physics, Chinese Academy of Science, Changchun 130033, China
[b] University of Chinese Academy of Science, Beijing 100049, China

ARTICLE INFO

Article history:
Received 23 May 2016
Received in revised form
12 July 2016
Accepted 16 July 2016
Available online 23 July 2016

Keywords:
Polarimetry
Refractive index estimation
Surface roughness estimation
Spectrometry

ABSTRACT

This paper presents a method to estimate refractive index and surface roughness simultaneously from multispectral and multiangular passive polarimetric measurements. Such a method has ties to passive remote sensing applications. Within the analysis, we use a previously derived expression for the degree of linear polarization, and a nonlinear least-squares algorithm to estimate the parameters of interest (i.e., refractive index and surface roughness) from the measured data. The results obtained from Monte Carlo simulations show that the estimation accuracy improves as the number of spectral channels and detection angles increase. It does so until the estimation accuracy reaches saturation. To take full advantage of the presented method, we also determine the most reasonable number of spectral channels and detection angles for our laboratory measurements using Monte Carlo simulations. Finally, after analyzing the experimental results for dielectric and metallic samples, we validate the effectiveness and advantages of the presented method to estimate refractive index and surface roughness for passive remote sensing.

1. Introduction

The polarization state of reflected light provides valuable information about surface features, shape, material composition, and surface roughness [1]. This makes polarimetric measurement a powerful tool in passive remote sensing, where the sensor relies on an unpolarized and usually uncontrolled illumination source like the sun. Passive polarimetric measurement techniques have been exploited in a number of applications such as target detection [2–4], shape estimation [5,6], material classification [7,8] and characterization [9–12].

One can use material characterization to estimate parameters of interest from a target. At optical wavelengths, refractive index and surface roughness are usually the parameters of interest within the analysis. Compared with other laboratory material characterization methods, the polarization-based material characterization technique is better for passive remote sensing. It requires one to solve forward and inverse problems to estimate the refractive index and surface roughness from polarimetric measurements. The forward problem involves deriving a reasonable model to describe the polarization state of the reflected light, and the inverse problem involves retrieving the parameters of interest from measured data with a numerical algorithm.

Early work on the estimation of refractive index and surface roughness for passive polarimetric remote sensing was published by Fetrow et al. [9]. Based on a simulation, they presented a method to estimate the complex refractive index of targets from long-wave infrared polarimetric measurements. Their studies showed that the surface roughness was a necessary quantity to be considered within the analysis in determining the refractive index through polarimetric measurements. To date, however, the surface roughness is ignored in most publications on polarization-based refractive index estimation.

Thilak et al. [10] presented a method to estimate complex refractive index and reflected angle from multiangular polarimetric measurements. Using the expression for the degree of linear polarization (DOLP) derived from a polarimetric bidirectional reflectance distribution function (pBRDF), they developed an effective algorithm based on nonlinear least-squares estimation. The main advantage of their method was that the result was largely invariant to the position of the source and the reflected angle [10]. Yet, they could only obtain the refractive index at a single wavelength. In addition, they ignored the diffuse component of reflection, which had the effect of lowering the DOLP.

Hyde et al. [11] proposed a novel remote-sensing material-characterization technique using passive polarimetric imagery degraded by atmosphere turbulence. The technique recovered refractive index from the turbulence-degraded polarimetric imagery using a variant of the blind-deconvolution algorithm. They

* Corresponding author at: Changchun Institute of Optics, Fine Mechanics and Physics, Chinese Academy of Science, Changchun 130033, China.
E-mail address: yangbin8086@163.com (Bin Yang).

http://dx.doi.org/10.1016/j.optcom.2016.07.042
0030-4018/

took diffuse reflection into account when deriving the DOLP expression. However, their polarimeter was not sensitive enough to make off-specular measurements. They only measured the DOLP specularly, making it difficult to estimate the surface roughness.

Sawyer et al. [12] developed a method for material characterization using multispectral polarimetric imagery. Their main contribution was that they introduced dispersion equations when estimating refractive index. The dispersion constants were determined via a nonlinear least-squares fit and then substituted into the dispersion equations to yield the refractive index. Nevertheless, they ignored diffuse scattering when deriving the DOLP expression. The measurements, fixed at a certain incident and reflected angle, also limited the estimation accuracy.

In this paper, we present a method to estimate the refractive index and surface roughness for passive remote sensing through multispectral and multiangular polarimetric measurements. In the aforementioned publications [10–12], they only used either multispectral measurements or multiangular measurements to estimate the parameters of interest. Here, we find that the estimation accuracy is improved by combining multispectral measurements with multiangular measurements. Using the method presented in this paper, we can also obtain more comprehensive information (i.e., the distribution of refractive index as a function of wavelength) about the target. The more accurate and more comprehensive information may be helpful in characterizing a material. Furthermore, we can estimate the surface roughness accurately using the presented method. By considering the surface roughness, we not only obtain the surface information about the target, but also reduce the impact of surface state on the refractive index estimation. In this way, the estimation accuracy of the refractive index is further improved. To take full advantage of the presented method, we find the most reasonable number of detection angles and spectral channels for our experiment through Monte Carlo simulations. The simulation and experimental results clearly show that the presented method is sufficient for the refractive index and surface roughness estimation.

The paper is structured as follows. Section 2 describes the derivation of the DOLP expression, which is based on a pBRDF model and dispersion equations, and introduces the estimation algorithm for the refractive index and surface roughness. Section 3 discusses and verifies the presented method with simulations. In Section 4, we summary and analyze our experimental results. Conclusions are presented in Section 5.

2. Methodology

To estimate the refractive index and surface roughness from polarimetric measurements, One must solve forward and inverse problems. Using a pBRDF model, the forward problem can be solved through a derived expression for the DOLP (topics of Sections 2.1 and 2.2). The inverse problem is usually solved by numerical techniques such as the nonlinear least-squares algorithm used in this paper, which is described in Section 2.3.

2.1. pBRDF Model

A pBRDF model is used to describe the radiance and polarization state of the light reflected from a material surface. In this paper, we use the model presented by Hyde et al. [13], which can characterize both the specular and diffuse components of reflection. The geometrical variables are illustrated in Fig. 1. We present some of the necessary equations for deriving an expression for the DOLP here. The interested reader can find more information in Ref. [13].

The pBRDF is defined as the ratio of the polarimetric reflected radiance to the polarimetric incident irradiance,

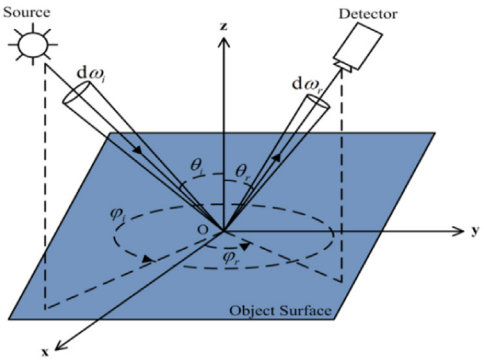

Fig. 1. pBRDF geometry. θ_i and θ_r are the incident zenith and reflected zenith angles, φ_i and φ_r are the incident azimuth and reflected azimuth angles, $d\omega_i$ and $d\omega_r$ are the incident solid and reflected solid angles, respectively.

$$\mathbf{F}(\theta_i, \theta_r, \phi) = \frac{d\mathbf{L}_r(\theta_r, \phi)}{\mathbf{L}_i(\theta_i)cos\theta_i d\omega_i}, \tag{1}$$

where $\phi = |\varphi_r - \varphi_i|$, $\mathbf{F}$ is the pBRDF Mueller matrix, $\mathbf{L}_i$ is the incident Stokes vector, and $\mathbf{L}_r$ is the reflected Stokes vector [13]. $\mathbf{F}$ can be represented as the sum of a specular component $\mathbf{F^s}$ and a diffuse component $\mathbf{F^d}$,

$$\mathbf{F} = \mathbf{F^s} + \mathbf{F^d}. \tag{2}$$

The specular component $\mathbf{F^s}$ is derived with the microfacet surface model proposed by Torrance and Sparrow [14]. This model assumes that a rough surface is comprised of a collection of microfacets randomly oriented whose angles are Gaussian distributed. Each microfacet is assumed to be a perfect reflector obeying the Fresnel equations. With these assumptions, the element in the jth row and kth column of the $\mathbf{F^s}$ can be expressed as

$$F^s_{jk}(\theta_i, \theta_r, \phi; \eta; \sigma) = \frac{\exp\left[-\tan^2\theta/\left(2\sigma^2\right)\right]}{8\pi\sigma^2 \cos\theta_i \cos\theta_r \cos^4\theta} \times G(\theta_i, \theta_r, \phi) \times M_{jk}(\theta_i, \theta_r, \phi; \eta), \tag{3}$$

where η is the complex refractive index, σ is the surface roughness, which is equivalent to the standard deviation of the surface slope [11], θ is the angle between the surface normal of a microfacet and the mean surface normal,

$$\theta = \arccos\left(\frac{\cos\theta_i + \cos\theta_r}{2\cos\beta}\right), \tag{4}$$

where

$$\beta = \frac{1}{2}\arccos(cos\theta_i cos\theta_r + \sin\theta_i \sin\theta_r cos\phi), \tag{5}$$

G is the visibility function, which describes the part of the illuminated facet that contributes to the scattered flux [14,15],

$$G(\theta_i, \theta_r, \phi) = min\left(1; \frac{2\cos\theta\cos\theta_r}{\cos\beta}; \frac{2\cos\theta\cos\theta_i}{\cos\beta}\right), \tag{6}$$

and M_{jk} is the element in the jth row and kth column of the Fresnel reflectance Mueller matrix.

The diffuse component $\mathbf{F^d}$ is derived with the directional hemispherical reflectance ρ_{DHR} [16]. It is given by

$$F^{d,PEC}_{00}(\theta_i, \sigma) = \frac{1}{\pi}[1 - \rho^{s,PEC}_{DHR}(\theta_i, \sigma)], \tag{7}$$

where the superscript PEC denotes that we are dealing with a

perfect reflecting surface, and the subscript 00 denotes the first row, first column element of a matrix.

The full pBRDF expression can be obtained through combining the specular component $\mathbf{F^s}$ with the diffuse component $\mathbf{F^d}$ [13],

$$F_{00}(\theta_i, \theta_r, \phi; \sigma; \eta) = F^s_{00}(\theta_i, \theta_r, \phi; \sigma; \eta) + \frac{1}{\pi}[1 - \rho^{s,PEC}_{DHR}(\theta_i, \sigma)] M_{00}(\theta_i, \theta_r, \phi; \eta) F_{jk}(\theta_i, \theta_r, \phi; \sigma; \eta) = F^s_{jk}(\theta_i, \theta_r, \phi; \sigma; \eta) \quad j, k \neq 0. \tag{8}$$

2.2. Derivation of DOLP

In this paper, we assume that the light source is unpolarized and scattering occurs in the principal plane (i.e., $\phi = \pi$). Furthermore, the circular polarization of the light reflected from most naturally illuminated surfaces can be ignored, which reduces M and F to 3×3 matrices [10]. After making these assumptions, the DOLP of the light is expressed as [13]

$$P(\theta_i, \theta_r; \eta; \sigma) = H(\eta; \beta) \times \frac{\Gamma(\theta_i, \theta_r; \theta; \sigma)}{\Gamma(\theta_i, \theta_r; \theta; \sigma) + \frac{1}{\pi}[1 - \rho^{s,PEC}_{DHR}(\theta_i; \sigma)]}, \tag{9}$$

where $\eta = n + ik$,

$$\Gamma(\theta_i, \theta_r; \theta; \sigma) = \frac{G(\theta_i, \theta_r, \pi)\exp\left[-\tan^2\theta/\left(2\sigma^2\right)\right]}{8\pi\sigma^2 \cos\theta_i \cos\theta_r \cos^4\theta}, \tag{10}$$

$$H(\eta; \beta) = \frac{R_s - R_p}{R_s + R_p}, \tag{11}$$

and R_s and R_p denote s-plane and p-plane Fresnel reflectances, respectively. When $\phi = \pi$, the expressions for θ and β reduce to

$$\theta = \frac{1}{2}(\theta_i - \theta_r)\ \beta = \frac{1}{2}(\theta_i + \theta_r). \tag{12}$$

Eq. (10) can be further simplified using the Fresnel's equations,

$$H(n, k; \beta) = \frac{2A\sin^2\beta \cos\beta}{A^2\cos^2\beta + \sin^4\beta + B^2\cos^2\beta}, \tag{13}$$

where the variables A and B are given by

$$A = \sqrt{\frac{\sqrt{C} + D}{2}} \quad B = \sqrt{\frac{\sqrt{C} - D}{2}}, \tag{14}$$

and

$$C = 4n^2k^2 + D^2, \tag{15}$$

$$D = n^2 - k^2 - \sin^2\beta. \tag{16}$$

Since we are interested in estimating η (i.e., n and k) from multispectral measurements, we must find a functional form for η whose parameters do not depend on wavelength. We can use dispersion equations for dielectric and metallic materials to transform η into variables independent of wavelength.

For dielectric materials, we use the Cauchy equation to describe the refractive index [17],

$$n = A_0 + \frac{A_1}{\lambda^2}, \tag{17}$$

where A_0 and A_1 are dispersion constants. The Cauchy equation can describe dielectric dispersion accurately at visible wavelengths. In addition, its simple form enhances the efficiency of estimation. We should note that the extinction coefficient k is ignored in the Cauchy equation, which is consistent with the characteristics of most dielectric materials. Combining Eqs. (13)–(17) and simplifying yields the full H expression for dielectric materials,

$$H = \frac{2\sqrt{D'}\sin^2\beta \cos\beta}{D'\cos^2\beta + \sin^4\beta} D' = \left(A_0 + \frac{A_1}{\lambda^2}\right)^2 - \sin^2\beta. \tag{18}$$

For metallic materials, the n and k in Eqs. (15) and (16) can be further derived by using the Drude model. The expression for complex refractive index η in the Drude model is given by

$$\eta^2 = 1 - \left(\frac{\omega_p^2}{\omega^2 + j\omega\tau^{-1}}\right), \tag{19}$$

where $\omega = 2\pi c/\lambda$, τ is the electron relaxation rate, and ω_p is the plasma frequency [18]. The ω_p and τ can be regarded as constants across a wide wavelength range for most metals. The advantage of the Drude model is that it is easy to break the η into expressions for the real part n and the imaginary part k [12]. Substituting Eq. (19) into Eqs. (13)–(16) and simplifying yields the full H expression for metallic materials,

$$H = \frac{2A''\sin^2\beta \cos\beta}{(A'')^2\cos^2\beta + \sin^4\beta + (B'')^2\cos^2\beta} A'' = \sqrt{\frac{\sqrt{C''} + D''}{2}} \quad B'' = \sqrt{\frac{\sqrt{C''} - D''}{2}} C'' = [\frac{\omega_P^2\tau}{\omega(1 + \omega^2\tau^2)}]^2 + (D'')^2 D'' = 1 - \frac{\omega_P^2\tau^2}{1 + \omega^2\tau^2} - \sin^2\beta. \tag{20}$$

The new DOLP expressions for dielectric and metallic materials can be obtained by substituting Eqs. (18) and (20) back into Eq. (9), respectively.

2.3. Refractive index and surface roughness estimation

We use a nonlinear least-squares algorithm to estimate the refractive index and surface roughness from the measured data. Firstly, the theoretical DOLP values P^t at multiple incident angles, reflected angles, and wavelengths are obtained using the pBRDF model. Then, the measured DOLP values P^m at those same incident angles, reflected angles, and wavelengths are compared with the theoretical DOLP values P^t to estimate the refractive index and surface roughness. The error between the P^t and P^m is defined as

$$\varepsilon = \sum_{l=1}^{L}\sum_{j=1}^{J}[P^t(\theta_{il}, \theta_{rl}; \lambda_j; E; \sigma) - P^m(\theta_{il}, \theta_{rl}; \lambda_j)]^2, \tag{21}$$

where L and J are the number of angles and spectral channels, respectively. The variable E denotes the constants (i.e., A_0 and A_1, or ω_p and τ) in the dispersion equations.

The values of E and σ can be identified as the estimation results when minimizing ε through the Levenberg–Marquardt algorithm [19]. The refractive index can then be obtained by substituting the constants A_0 and A_1, or ω_p and τ into the dispersion equations.

Noteworthy is that we use $L \times J$ data points, L angles and J spectral channels, to estimate the refractive index and surface roughness. It means that more constraints are imposed on the process of estimation, which may yield more accurate estimation results than only using either L multiangular measured data points or J multispectral measured data points. Through the presented method, we can recover the refractive index at J different wavelengths simultaneously, instead of only one value at a single wavelength, which allows us to obtain more comprehensive information about the target. In Eq. (21), the surface roughness σ serves as an independent variable in the model of the theoretical DOLP. By doing so, we can extract the surface characteristic and

Please cite this article as: Bin Yang, et al., Optics Communications (2016), http://dx.doi.org/10.1016/j.optcom.2016.07.042

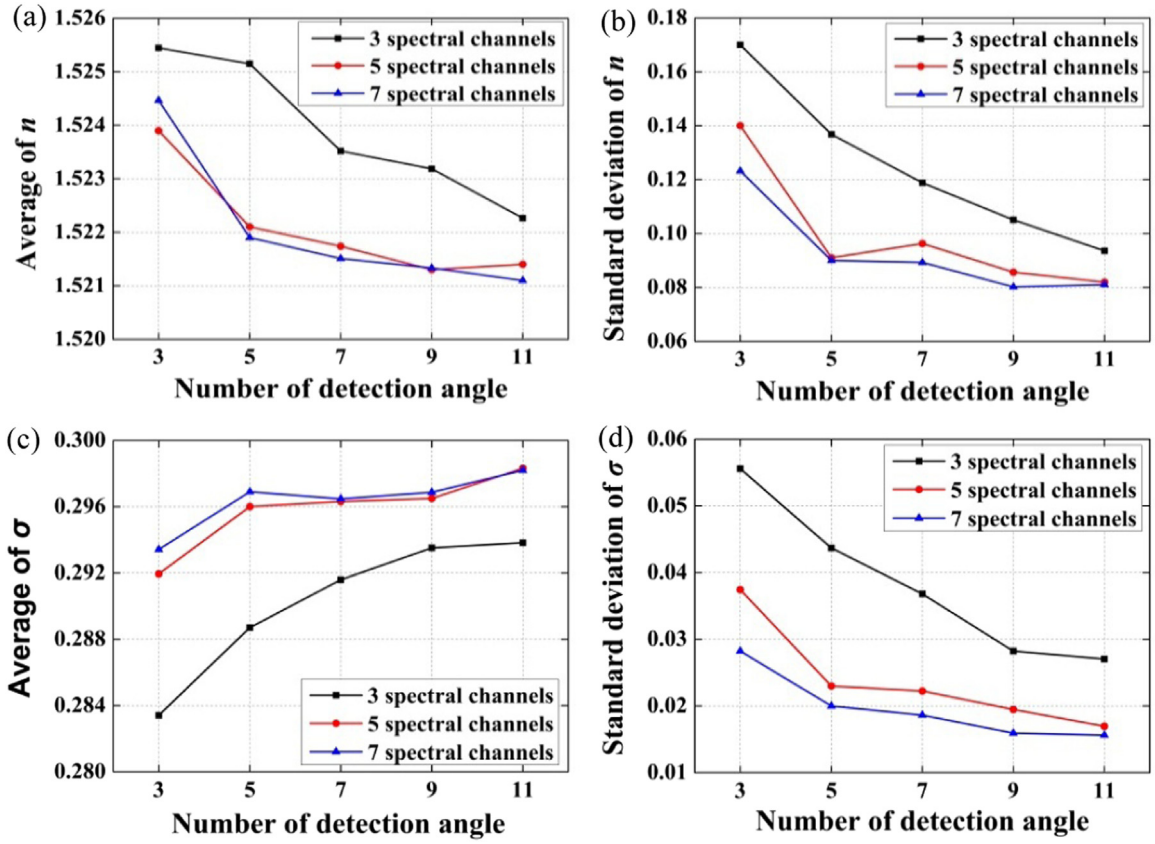

Fig. 2. Simulation results for a dielectric material (a, b) the averages and standard deviations of the real refractive index; (c, d) the averages and standard deviations of the surface roughness. The input dispersion constants are $A_0 = 1.5046$ and $A_1 = 0.0042$, and the input surface roughness is $\sigma = 0.3$. According to the Cauchy equation, the input refractive index is $n = 1.5185$ at 550 nm. The results are achieved from 1000 Monte Carlo trials.

reduce the impact of surface roughness on the refractive index estimation, which effectively improves the accuracy of the material characterization.

3. Simulation analysis

In this section, we analyze and validate the presented method with Monte Carlo simulations. Synthetic data for simulations are produced using the pBRDF model in Section 2 with specific θ_i, θ_r, σ, λ, and dispersion constants. The value of θ_i is fixed at 45°, while a series of values for θ_r (i.e., detection angle) are used in the simulations. We use 3, 5, 7, 9, and 11 detection angles, 3, 5, and 7 spectral channels for different simulations, respectively. For each simulation, θ_r is always uniformly distributed between 40° and 60°, while λ is always uniformly distributed between 450 nm and 650 nm. With that said, when the number of detection angles is 3, 5, 7, 9, and 11, the step sizes of detection angles will be 10°, 5°, 3.3°, 2.5°, and 2°, respectively. When the number of spectral channels is 3, 5, and 7, the step sizes of spectral channels will be 100 nm, 50 nm, and 33 nm, respectively.

In order to analyze the robustness of our method to noise, white Gaussian noise is added to the synthetic data. The standard deviations of the noises are equal to 2% of the synthetic DOLP values, which is consistent with the accuracy of our laboratory equipment in the selected bands. Then, the Levenberg–Marquardt solver is used to estimate the refractive index and surface roughness from the noisy inputs. The simulation analyses are performed for both dielectric and metallic materials.

Fig. 2 shows the simulation results for a dielectric material, which is assumed to be BK7 glass. We provide the simulation results at 550 nm. From the averages and standard deviations of the estimation results, we conclude that the refractive index and surface roughness can be retrieved from the noisy simulated data. We also see that the results with a fixed number of detection angles (i.e., 3, 5, 7, 9, or 11) become more accurate as the number of spectral channels increases. It does so until the estimation accuracy reaches saturation. More specifically, there is a significant improvement in the estimation accuracy when the number of spectral channels increases from 3 to 5. However, no more obvious improvement appears as the number increases from 5 to 7 due to the noise floor. For a fixed number of spectral channels (i.e., 3, 5, or 7), it is also clear that the estimation accuracy improves with the number of detection angles increasing until a saturation point.

To take full advantage of the presented method, the most reasonable number of detection angles and spectral channels are determined on the basis of the saturation points. By analyzing the trends of the curves in Fig. 2, the most reasonable number of spectral channels and detection angles are determined to be 5 and 5, which is under the simulated noise level. There is little improvement in the estimation accuracy with more measurements, while the cost increases considerably. When recovering the refractive index and surface roughness from the measured data, the saturation points are determined by the accuracy of the measurements. Because the noise levels in the simulations are consistent with the accuracy of our experimental equipment, we use 5 spectral channels and 5 detection angles to measure the dielectric samples.

Fig. 3 shows the estimations for a metallic material, assumed to be aluminium. We also provide the simulation results at 550 nm. When estimating a metallic material, we do not ignore the imaginary part of the refractive index. We find that the averages grow

Please cite this article as: Bin Yang, et al., Optics Communications (2016), http://dx.doi.org/10.1016/j.optcom.2016.07.042

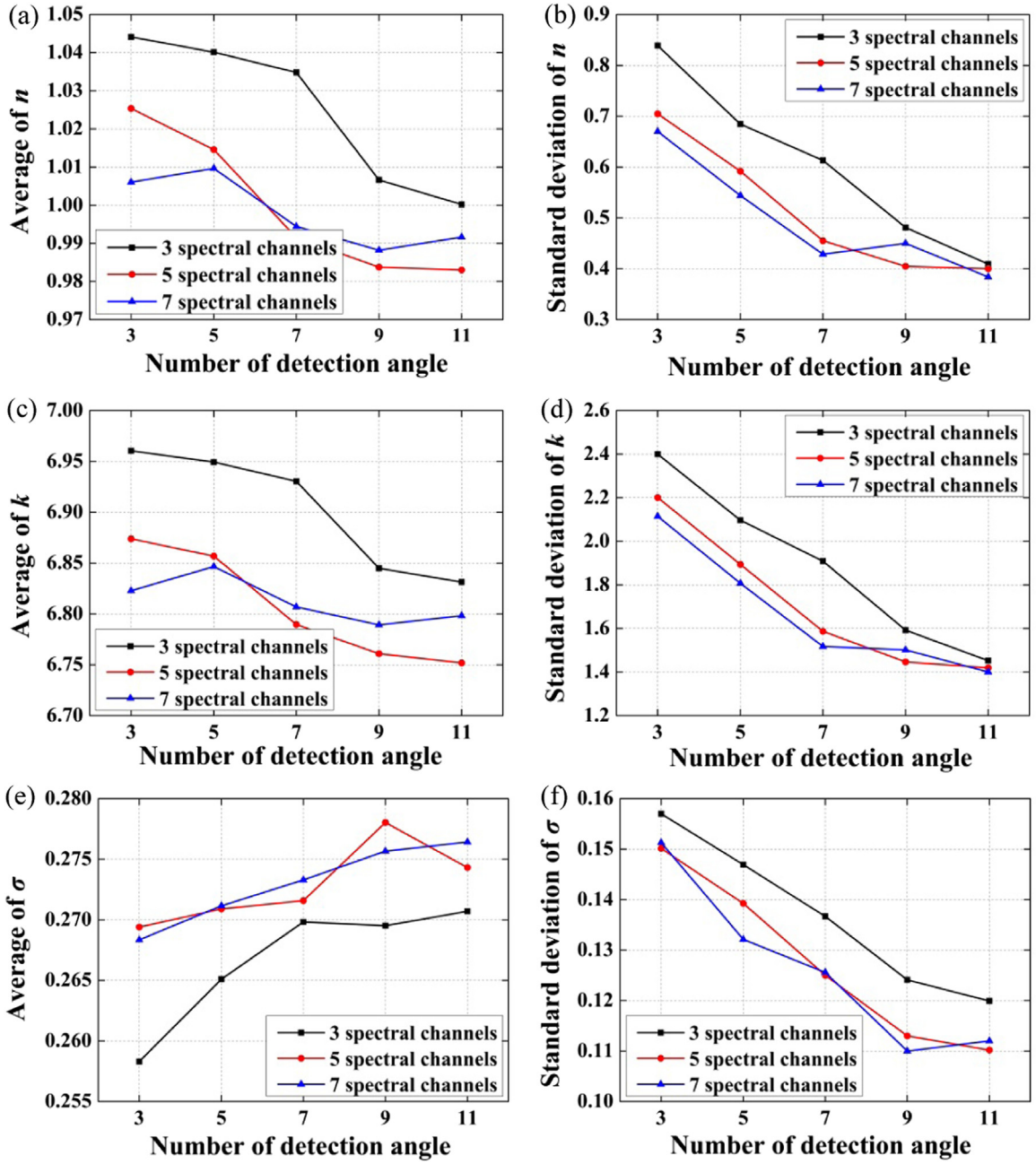

Fig. 3. Simulation results for a metallic material (a, b) the averages and standard deviations of the real refractive index; (c, d) the averages and standard deviations of the imaginary refractive index; (e, f) the averages and standard deviations of the surface roughness. The input dispersion constants are $\omega_p = 2.39 \times 10^{16}$ rad/s and $\tau = 1.02 \times 10^{-15}$ s, and the input surface roughness is $\sigma = 0.3$. According to the Drude model, the input refractive index is $n = 0.958$ and $k = 6.69$ at 550 nm. The results are achieved from 1000 Monte Carlo trials.

closer to the true values, and the standard deviations become smaller with the number of spectral channels and detection angles increasing until the estimation accuracy saturates. According to the results, the most reasonable number of spectral channels is 5, and the most reasonable number of detection angles is 9. These results are also adopted in our experiments when measuring the metallic samples.

The simulations for the dielectric and metallic materials suggest that there are two main factors influencing the accuracy of the estimation results. One is the number of spectral channels and detection angles, which are found through the above simulations. The other is the noise level dependent on the accuracy of the measurement, and one can perform further study on the presented method by developing more accurate equipments.

4. Experimental results

In our experiment, the DOLP of the reflected light is measured with the Northeast Normal University Laboratory Goniospectrometer System (NENULGS), shown in Fig. 4. The NENULGS consists of a goniometer, a tungsten halogen lamp and an Analytical Spectral Devices FieldSpec 3 (ASD FS3) spectroradiometer. Using the goniometer, one can perform measurements with zenith angles ranging from $-90°$ to $90°$ and azimuth angles ranging from $0°$ to $360°$. The tungsten halogen lamp, which is attached to a $90°$ arc with a 1.5 m radius, is used as the source of unpolarized illumination. Spectral polarized reflectance measurements are performed using the ASD FS3 spectroradiometer. In order to improve the signal to noise ratio (SNR) in our experiments, we group ten

Please cite this article as: Bin Yang, et al., Optics Communications (2016), http://dx.doi.org/10.1016/j.optcom.2016.07.042

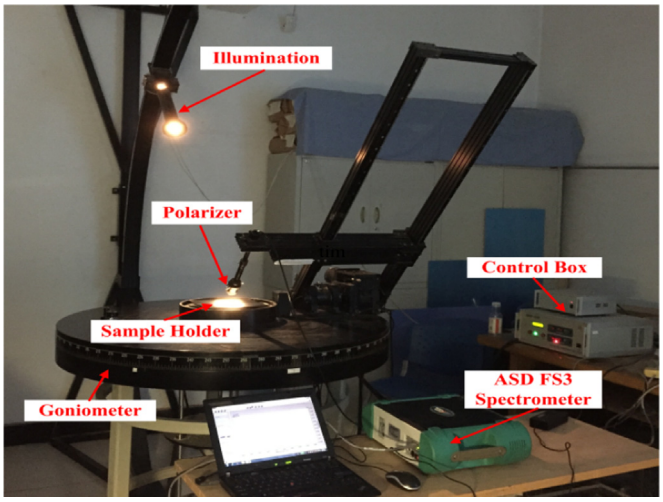

Fig. 4. Photograph of the NENULGS used in this experiment.

neighboring pixels of the spectroradiometer. To measure the radiance in different polarization directions, a calcite Glan–Thomson prism, which allows for rotation from 0° to 360° in 1° increments, is used in front of the fiber-optic detector of the spectroradiometer. More details about the NENULGS can be found in Ref. [20].

The samples in our experiments are BK7 glass, quartz, a roughened aluminium plate, and a roughened copper plate, shown in Fig. 5. The diameters of the BK7 glass and the quartz are 80 cm and 70 cm, respectively, and their thicknesses are both 10 cm. The sizes of the aluminium and copper plates are 11 cm × 11 cm, and their thicknesses are 5 cm. For the BK7 glass, quartz and roughened aluminium plate, the selected measuring wavelengths are 450 nm, 500 nm, 550 nm, 600 nm, and 650 nm, while for the roughened copper plate, they are 700 nm, 750 nm, 800 nm, 850 nm, and 900 nm. To guarantee the geometry, shown in Fig. 1, we used a leveler with a bubble to level the sample surfaces in our experiments.

The size of the field of view is 8° when measuring all the samples. We must change the sensor zenith angle in the measurements, which leads to minor variations in the size of detection. The elongated region under inspection at larger view zenith angles fits completely inside the homogenous part of the illumination. Since the values of surface roughness are approximately equal in different parts of each sample and the illumination is uniform, the effect of the minor variations on the average values of the measured surface roughness can be ignored.

The DOLP is derived from the first three components of the Stokes vector, given the symbols I, Q, and U. In this paper, the parameters I, Q, and U are calculated by the light intensity measured from four directions of the analyzer: 0°, 45°,90°, and 135° [21]. The meridional plane of the instrument is taken as the reference plane for the analyzer (i.e., the Glan–Thomson prism). The expressions for I, Q, and U are given by [22]

$$I = \frac{1}{2}(I_0 + I_{45} + I_{90} + I_{135})Q = I_0 - I_{90}U = I_{45} - I_{90}, \tag{22}$$

where I_0, I_{45}, I_{90}, and I_{135} are the light intensities measured with the analyzer oriented at 0°, 45°, 90°, and 135°. The DOLP is given by

$$\mathrm{DOLP} = \frac{\sqrt{Q^2 + U^2}}{I}. \tag{23}$$

Fig. 6 shows the measured and estimated DOLP values of the light reflected from the BK7 glass and quartz, in which the DOLP values are provided by varying the detection angle at five different wavelengths. In our experiments, the incident angle is fixed at 45°. To improve SNR, we measure the DOLP in a region where the signal is much larger than the noise. After a preliminary experiment, we find that the usable areas of the BK7 glass and quartz samples only extend over about a 10° range. As a result, we are forced to choose the detection angles between 40° and 50°, and adjust the step size to 2.5°. We see that the estimated DOLP values match well with the measured DOLP values in every spectral channel, which illustrates the effectiveness of our method for estimating the refractive index.

Tables 1 and 2 list the results of refractive index for the BK7 glass and quartz. We ignore the imaginary part of refractive index for the dielectric materials in visible spectrum. We obtain the distribution of the refractive index as a function of wavelength, which contributes to characterizing the target. In addition, the estimation errors for the BK7 glass and quartz are about 4% as compared with the reference data [23]. Sawyer et al. [12] also estimated the refractive index of BK7 glass. The errors of their results were 6.47% at 450 nm and 6.09% at 550 nm. Compared with these, we find that the accuracy of the results in this paper improves, which mainly because we use the multiangular measurements within our estimate. Furthermore, there is a little difference between the refractive index of the BK7 glass and quartz, yet our method can still distinguish between the two. The high estimation accuracy of the refractive index illustrates that the presented method has much utility in the field of material characterization.

Fig. 7 shows the measured and estimated DOLP values for the metallic surfaces. We keep the incident angle at 45° in the experiments. By using the same method as for the dielectric samples, we see that the usable areas of the aluminium plate and copper plate extend over about a 20° range. Therefore, we choose the detection angles from 40° to 60° with a step size of 2.5°, which is consistent with the simulations. For clarity, we should mention that the Drude model is not appropriate for metals near their absorption band. Since the transition energy of copper is about 2.2eV, which corresponds to a wavelength of 560 nm [18], the selected wavelengths for the copper plate are adjusted to 700 nm,

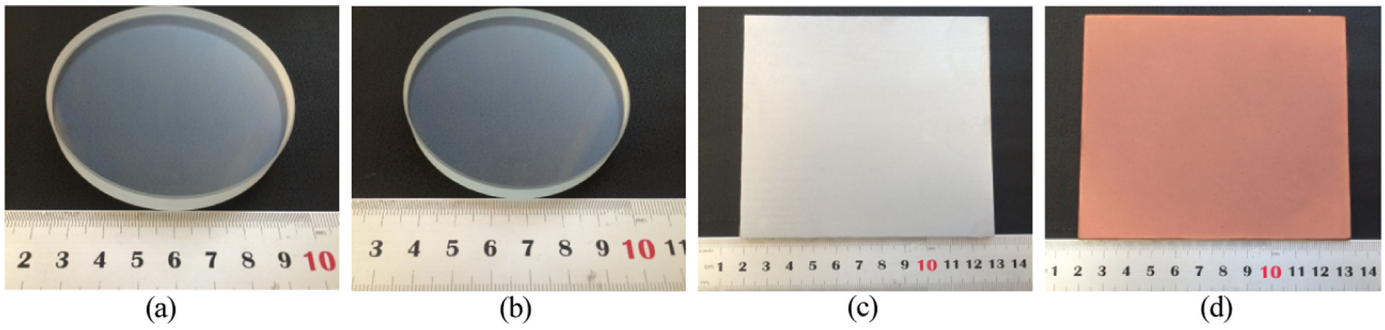

Fig. 5. Photographs of the samples used in this experiment (a) BK7 glass; (b) quartz; (c) aluminium plate; (d) copper plate.

Please cite this article as: Bin Yang, et al., Optics Communications (2016), http://dx.doi.org/10.1016/j.optcom.2016.07.042

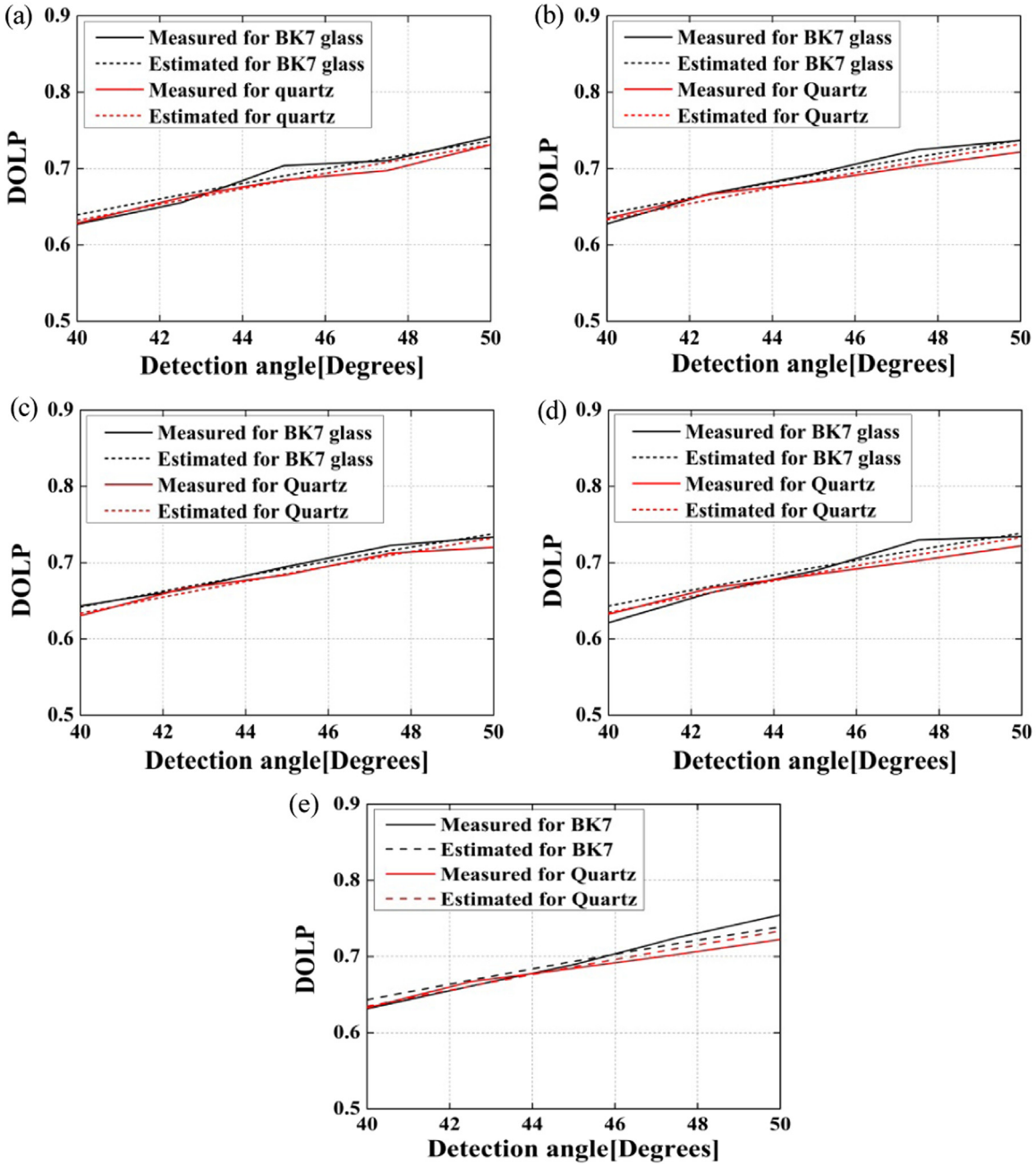

Fig. 6. Measured and estimated DOLP plots for the dielectric samples. Black is for the BK7 glass and red is for the quartz. The center wavelengths of the spectral channels used for the BK7 glass and quartz are: (a) 450 nm; (b) 500 nm; (c) 550 nm; (d) 600 nm; (e) 650 nm.

Table 1
Estimated refractive index and percent error for the BK7 glass.

Wavelength (nm)	Estimated n	Reference n	Error of n (%)
450	1.588	1.525	4.13
500	1.580	1.521	3.88
550	1.575	1.519	3.69
600	1.571	1.516	3.63
650	1.568	1.515	3.50

Table 2
Estimated refractive index and percent error for the quartz.

Wavelength (nm)	Estimated n	Reference n	Error of n (%)
450	1.628	1.552	4.67
500	1.622	1.549	4.50
550	1.618	1.546	4.45
600	1.615	1.544	4.40
650	1.613	1.542	4.40

750 nm, 800 nm, 850 nm, and 900 nm. We observe that, compared with the dielectric surfaces, more fluctuations appear on the curves of the experimental DOLP values for the aluminium and copper samples. The main reason is that the s-plane Fresnel reflectance R_s and p-plane Fresnel reflectance R_p of metallic materials are approximately equal over most observation conditions, leading to difficulty in the DOLP measurement. This is also a critical factor influencing the estimation accuracy for metallic samples.

Table 3 lists the estimated results of refractive index for the aluminium plate. We find that the estimated values do not agree

Please cite this article as: Bin Yang, et al., Optics Communications (2016), http://dx.doi.org/10.1016/j.optcom.2016.07.042

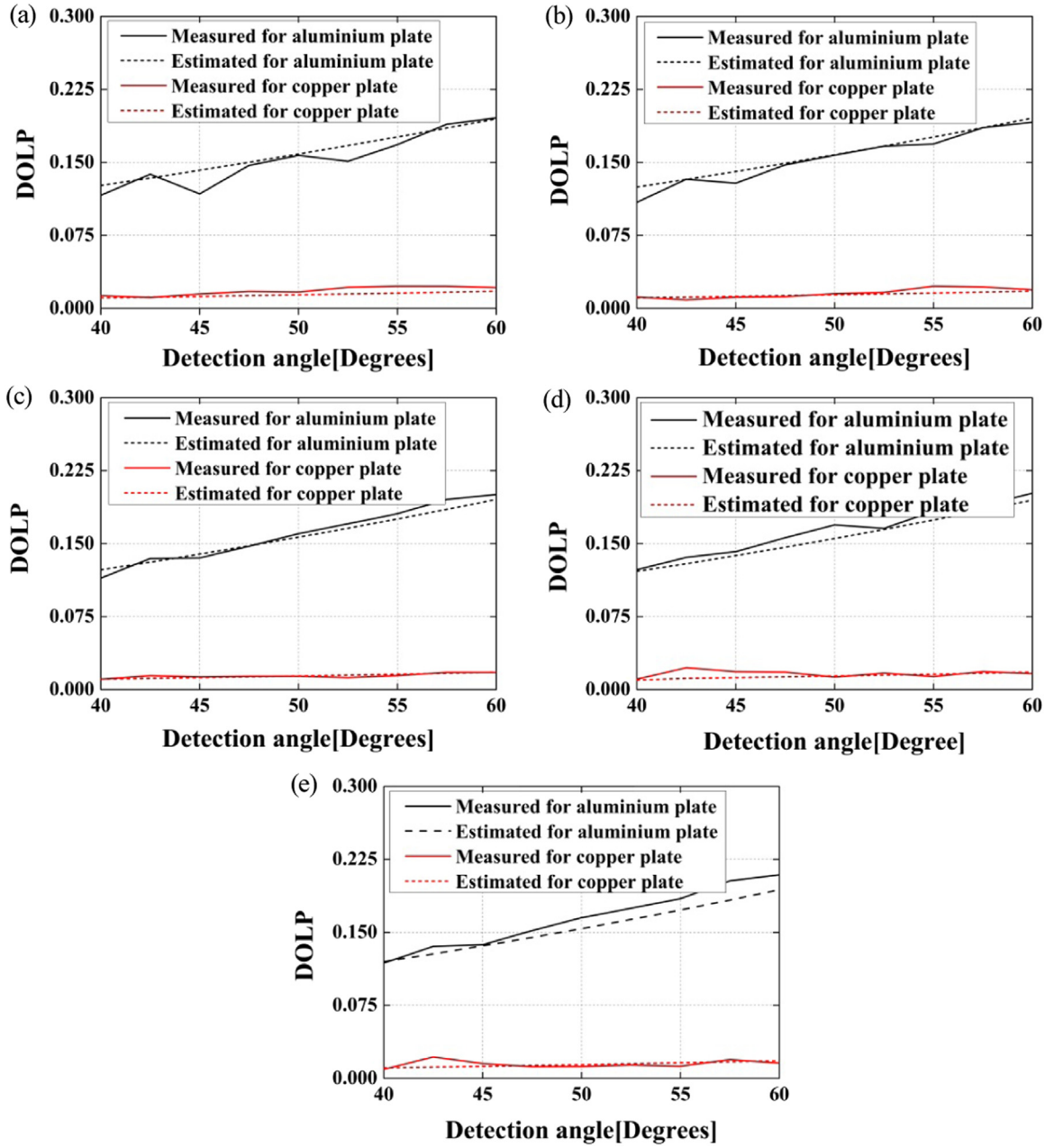

Fig. 7. Measured and estimated DOLP plots for the metallic samples. Black is for the aluminium plate and red is for the copper plate. The center wavelengths of the spectral channels used for the aluminium plate are: (a) 450 nm; (b) 500 nm; (c) 550 nm; (d) 600 nm; (e) 650 nm, while for the copper plate are: (a) 700 nm; (b) 750 nm; (c) 800 nm; (d) 850 nm; (e) 900 nm.

with the reference data [24]. The differences may be related to the surface characteristic of aluminium, which is easily oxidized. The coating of oxide on the aluminium surface changes the DOLP of the reflected light. As a result, the estimated values deviate from the true refractive index of aluminium. In addition, we note that the estimated results are close to the reference data for alumina [23]. It indicates that the presented method has a potential application in detecting the oxidation rate of aluminium. Table 4 lists the results for the copper plate. The errors of our estimated n and k are mostly less than 10% compared with the reference values [23], while the errors of the results obtained by Thilak et al. are about 30% for n and 10% for k at 650 nm [10]. The more accurate

Table 3
Estimated refractive index and percent error for the aluminium plate.

Wavelength (nm)	Estimated n	Reference n	Error of n (%)	Estimated k	Reference k	Error of k (%)
450	1.864	0.618	201.6	3.579	5.47	34.6
500	2.013	0.769	161.8	3.730	6.08	38.9
550	2.158	0.958	125.3	3.872	6.69	42.1
600	2.300	1.020	125.5	4.005	7.26	44.8
650	2.437	1.470	65.8	4.132	7.79	47.0

Please cite this article as: Bin Yang, et al., Optics Communications (2016), http://dx.doi.org/10.1016/j.optcom.2016.07.042

Table 4
Estimated refractive index and percent error for the copper plate.

Wavelength (nm)	Estimated n	Reference n	Error of n (%)	Estimated k	Reference k	Error of k (%)
700	0.205	0.214	4.39	4.556	4.158	8.74
750	0.234	0.231	1.28	4.895	4.607	5.88
800	0.265	0.250	5.66	5.232	5.034	3.78
850	0.299	0.270	9.70	5.568	5.442	2.26
900	0.334	0.291	12.87	5.903	5.829	1.25

Table 5
Estimated and measured values of surface roughness for the samples.

Sample	Estimated σ (rad)	Measured σ_s (rad)
Bk7 glass	0.063	0.084
Quartz	0.051	0.076
Aluminium plate	0.434	0.406
Copper plate	0.397	0.368

estimation results further prove the effectiveness of the presented method to estimate the refractive index for metallic materials. More importantly, we find that the two different kinds of metallic materials are easily distinguished through the method presented here, which is critical for classifying materials by passive polarimetric remote sensing.

Another advantage of our work is that we estimate the surface roughness simultaneously with the refractive index of the sample, which provides us with the surface characteristic of the target. The DOLP of the light reflected from the same kind of material will vary with the surface state. Since our method estimates the parameters of interest from the DOLP measurements, we must take the surface roughness into account.

Before the estimation, we used a Taylor Hobson PGI-830 surface profiler to measure the surface roughnesses of the samples. Based on phase grating interferometry technology, the instrument has a resolution of 0.8 nm. The measurements generated a data set of 50,000 surface points for each sample. We assume that the surface heights are Gaussian distributed and Gaussian correlated [25]. The data sets were then analyzed to determine the root-mean-square (rms) roughnesses in meters and surface correlation lengths of the samples. The measured standard deviation of surface slope σ_s in radians is given by

$$\sigma_s = \frac{\sqrt{2}\sigma_h}{l}, \tag{24}$$

where σ_h is the rms roughness in meters, l is the surface correlation length of the samples.

Table 5 lists the values of the estimated σ and measured σ_s for the samples. The surface roughness can be estimated accurately using the method presented here, especially for the rougher targets (i.e., the roughened copper and aluminium plates). For a smooth surface, the diffuse reflection is very weak, which leads to difficulty in estimating the surface roughness. Nevertheless, we find out the difference between the surface roughnesses of the BK7 glass and quartz. The estimated values can be taken as a roughness comparison criterion between different surfaces. More importantly, the estimated σ can describe the diffuse component of reflection, which makes the calculated DOLP through the pBRDF model more accurate. In this way, we reduce the impact of surface state on the refractive index estimation. It is one of the main reasons why the presented method can improve the estimation accuracy of the refractive index.

5. Conclusions

In this paper, we present a method to estimate refractive index and surface roughness from multispectral and multiangular passive polarimetric measurements. The method uses a previously derived DOLP model, and estimates the parameters of interest through the Levenberg–Marquardt algorithm. The Monte Carlo simulation results indicate that the estimation results become more accurate as the number of spectral channels and detection angles increase until the estimation accuracy saturates. After further analyzing the simulation results, we determine the most reasonable number of spectral channels and detection angles to be 5 and 5 for a dielectric surface, and 5 and 9 for a metallic surface. In addition, the experimental results validate the effectiveness and advantages of the presented method. Through the estimated refractive index, a certain material can be distinguished from others. The estimated surface roughness can also accurately provide us with the surface characteristic of the target.

Our work shows that more accurate and more comprehensive information about the target can be obtained through the presented method. Firstly, the accuracy of refractive index estimation is improved by combining multispectral measurements with multiangular measurements and reducing the impact of surface roughness on the refractive index estimation. Secondly, the distribution of refractive index as a function of wavelength can be estimated from the multispectral data. Furthermore, the surface characteristic of the target can be obtained accurately by estimating its roughness. In general, with a more accurate and more comprehensive estimation, the presented method gains an obvious advantage in the field of material characterization for passive remote sensing.

Acknowledgments

This work was supported by the National High Technology Research and Development Program of China [Grant number 2011AA12A103]; and the National Natural Science Foundation of China [Grant number 61505199]. The authors would like to thank the anonymous reviewers for their useful comments and critical remarks which helped to improve this paper.

Appendix A. Supporting information

Supplementary data associated with this article can be found in the online version at http://dx.doi.org/10.1016/j.optcom.2016.07.042.

References

[1] J.S. Tyo, D.L. Goldstein, D.B. Chenault, J.A. Shaw, Review of passive imaging polarimetry for remote sensing applications, Appl. Opt. 45 (2006) 5453–5469.
[2] F.A. Sadjadi, C.S.L. Chun, Remote sensing using passive infrared Stokes parameters, Opt. Eng. 43 (2004) 2283–2291.
[3] F. Goudail, P. Terrier, Y. Takakura, L. Bigué, F. Galland, V. DeVlaminck, Target detection with a liquid-crystal-based passive Stokes polarimeter, Appl. Opt. 43 (2004) 274–282.
[4] M.G. Gartley, W. Basener, Topological anomaly detection performance with multispectral polarimetric imagery, Proc. SPIE 7334 (2009) 73341O.
[5] G.A. Atkinson, E.R. Hancock, Recovery of surface orientation from diffuse

polarization, IEEE Trans. Image Process 15 (2006) 1653–1664.
[6] C. Stolz, M. Ferraton, F. Meriaudeau, Shape from polarization: a method for solving zenithal angle ambiguity, Opt. Lett. 37 (2012) 4218–4220.
[7] L.B. Wolff, Polarization-based material classification from specular reflection, IEEE Trans. Pattern Anal. Mach. Intell. 12 (1990) 1059–1071.
[8] S. Tominage, A. Kimachi, Polarization imaging for material classification, Opt. Eng. 47 (2008) 123201.
[9] M.P. Fetrow, D.L. Wellems, S.H. Sposato, K.P. Bishop, T.R. Caudill, M.L. Davis, E. R. Simrell, Results of a new polarization simulation, Proc. SPIE 4481 (2002) 149–162.
[10] V. Thilak, D.G. Voelz, C.D. Creusere, Polarization-based index of refraction and reflection angle estimation for remote sensing applications, Appl. Opt. 46 (2007) 7527–7536.
[11] M.W. Hyde IV, J.D. Schmidt, M.J. Havrilla, S.C. Cain, Determining the complex index of refraction of an unknown object using turbulence-degraded polarimetric imagery, Opt. Eng. 49 (2010) 126201.
[12] M.A. Sawyer, M.W. Hyde IV, Material characterization using passive multispectral polarimetric imagery, Proc. SPIE 8873 (2013) 88730Y.
[13] M.W. Hyde IV, J.D. Schmidt, M.J. Havrilla, A geometrical optics polarimetric bidirectional reflectance distribution function for dielectric and metallic surfaces, Opt. Express 17 (2009) 22138–22153.
[14] K.E. Torrance, E.M. Sparrow, Throry for off-specular reflection from roughened surfaces, J. Opt. Soc. Am. 57 (1967) 1105–1114.
[15] J.F. Blinn, Models of light reflection for computer synthesized pictures, in: Proceedings of the 4th Annual Conference on Computer Graphics and Interactive Techniques, New York, USA, 1977.
[16] R.G. Priest, S.R. Meier, Polarimetric microfacet scattering theory with applications to absorptive and reflective surfaces, Opt. Eng. 41 (2002) 988–993.
[17] L.Z. Cai, Optics, 3rd ed., Science, Beijing, 2007.
[18] M. Fox, Optical Properties of Solids, Oxford University, Oxford, 2001.
[19] K. Madsen, H.B. Nilsen, O. Tingleff, Methods for Non-linear Least Squares Problems, Technical university of Denmark, Copenhagen, 2004.
[20] Z.Q. Sun, Z.F. Wu, Y.S. Zhao, Semi-automatic laboratory goniospectrometer system for performing multi-angular reflectance and polarization measurements for natural surfaces, Rev. Sci. Instrum. 85 (2014) 014503.
[21] F. Goudail, A. Beniere, Estimation precision of the degree of linear polarization and of the angle of polarization in the presence of different sources of noise, Appl. Opt. 49 (2010) 683–693.
[22] D.A. Talmage, P.J. Curran, Remote sensing using partially polarized light, Int. J. Remote Sens. 1 (1986) 47–64.
[23] G. Boisset, Luxpop-Thin Film and Bulk Index of Refraction and Photonics Calculations. ⟨http://www.luxpop.com/⟩.
[24] E.D. Palik, Handbook of Optical Constants of Solids, Academic, San Diego, 1985.
[25] P. Beckmann, A. Spizzichino, The Scattering of Electromagnetic Waves from Rough Surfaces, Pergamon, Oxford, 1963.

Please cite this article as: Bin Yang, et al., Optics Communications (2016), http://dx.doi.org/10.1016/j.optcom.2016.07.042